minerals

MDPI

Article

Zircon U-Pb Age and Geochemistry of Yamusi Granodiorite in the Eastern Part of the Qilian Orogen, China

Lei Pei [1,2], Xianzhi Pei [1,2,*], Yu Zhang [1], Ruibao Li [1,2], Youxin Chen [1,2], Zuochen Li [1,2], Chengjun Liu [1,2] and Meng Wang [1,2]

[1] School of Earth Science and Resource, Chang'an University, Xi'an 710054, China; peilei.1989@163.com (L.P.)
[2] Key Laboratory of Western Mineral Resource and Geological Engineering, Ministry of Education, Xi'an 710054, China
* Correspondence: peixzh@chd.edu.cn

Abstract: Yamusi granodiorite in the eastern part of the Qilian Orogen consists mainly of gneissic granodiorite. Researchers have studied other nearby rock masses, and many studies, such as those focusing on the zircon U-Pb age chronology and geochemistry of Yamusi granodiorite, still need to be completed. We obtained a new LA–ICP–MS zircon U-Pb age of 480.3 ± 1.3 Ma for Yamusi granodiorite, which suggested that it was formed during the early Ordovician period. The whole-rock geochemical data show that this granodiorite is relatively rich in Na and poor in K (K_2O/Na_2O = 0.40–0.73). The granodiorite is metaluminous–weakly peraluminous and can be classified as medium-K calc-alkaline granite. It yields high Sr/Y ratios (35.17–53.78) and low Yb (<18 ppm) and Y (1.8 ppm) contents, an Mg# value of <45, and high La/Y ratios (2.9–13.4, mean = 5.76). The trace element compositions of the granodiorite are characterized by positive large-ion lithophile elements (LILEs; e.g., Cs, Rb, and Ba) and negative high-field-strength element (HFSE; e.g., Nb, Ta, and Ti) anomalies, similar to arc magmatic rocks. There is clear fractionation between the light and heavy rare earth elements (REEs), with $(La/Yb)_N$ ratios of 1.77–9.03 (mean = 3.88). The petrogenesis research suggests that the granodiorite originated mainly from the partial melting of the mafic lower crust, with a minor mantle-derived component. Based on the regional geological setting, we suggest that the Yamusi granodiorite was formed during the northward subduction of the Proto-Tethyan oceanic crust to form an intracontinental arc.

Keywords: Qilian Orogen; island arc magmatic rocks; Yamusi granitoid; Proto-Tethys; adakite

check for updates

Citation: Pei, L.; Pei, X.; Zhang, Y.; Li, R.; Chen, Y.; Li, Z.; Liu, C.; Wang, M. Zircon U-Pb Age and Geochemistry of Yamusi Granodiorite in the Eastern Part of the Qilian Orogen, China. *Minerals* **2023**, *13*, 677. https://doi.org/10.3390/min13050677

Academic Editor: David Lentz

Received: 20 March 2023
Revised: 10 May 2023
Accepted: 10 May 2023
Published: 15 May 2023

1. Introduction

The extensive ophiolites and island arc magmatism in western China have recorded a complex evolutionary history from the Proto-Tethys to the Paleo-Tethys Oceans with the involvement of multiple microcontinents, ocean basins, and island arcs [1–14] (Figure 1). Recent studies have reported data from early Paleozoic magmatic and volcanic rocks [15–19] and high-pressure–ultrahigh-pressure (HP–UHP) metamorphism within the northern Qaidam Basin [20–27]. Wu et al. [16–19] studied the early Paleozoic rocks in this belt and concluded that the rocks on the northern margin of the Qaidam Basin could be subdivided into four age groups and different tectonic environments (early middle Ordovician (460–475 Ma), late Ordovician (440–450 Ma), late Silurian to early Devonian (395–410 Ma), and late Devonian (370–385 Ma). The HP–UHP metamorphic belt on the northern margin of the Qaidam Basin–South Qilian tectonic belt is composed mainly of granitic gneisses and pelitic gneisses with continental crustal rocks as the protoliths, and the gneisses often contain variable amounts of eclogitic and ultramafic clasts. The ages of the zircon grains in these gneisses, eclogites, and ultramafic rocks show that they first underwent HP metamorphism below the stability field of coesite at 476–445 Ma, followed by ultrahigh-pressure metamorphism at 440–421 Ma, with the early HP metamorphism being related to oceanic subduction and the later UHP metamorphism representing continental subduction (i.e., the continental subduction of the Qaidam continental lithosphere) [28]. In addition, Shi et al. [29], Xu et al. [15], and Xia et al. [28] suggested that the early Paleozoic (515–485 Ma) arc volcanic rocks of the Tanjianshan Group along the north of the HP–UHP metamorphic belt were products of the arc volcanism induced by the northward subduction of the oceanic crust beneath the northern margin of the Qaidam Basin.

Studies on the early Paleozoic magmatism in the eastern part of the South–Central Qilian Orogen have focused primarily on the magmatism associated with collisional and post-collisional environments, and Zhang et al. [30–33] studied the mafic–ultramafic rocks (440–449 Ma) in the interior of the Hualong micro-massif and concluded that they were formed under a post-collisional extensional regime. Yong et al. [34] studied Dongjiazhuang granite (446.9 ± 1 Ma) (LA–ICP–MS zircon U-Pb age) and the Xindian intrusion (454 ± 5 Ma), and Yang et al. [35] studied the Jishishan intrusion in the eastern Central Qilian Orogen (452 ± 5 Ma), and their results suggested that these granites were formed in a post-collisional environment. Guo et al. [36] studied Rumanshan granite (452 ± 1.8 Ma) in the Hualong area of the South Qilian Orogen and concluded that it is I-type granite. Previous studies have focused mainly on the central and western parts of the South–Central Qilian orogenic belts, whereas the rocks associated with subduction during the early Paleozoic in the eastern part of the South–Central Qilian orogenic belts have been less studied. Therefore, this study is of great significance for research on Yamusi gneissic granodiorite.

Yamusi gneissic granodiorite is located in the eastern part of the South–Central Qilian orogenic belts and is crucial to the understanding of the northward subduction and accretion of the early Paleozoic Proto-Tethyan oceanic crust (Figure 1). At present, research on Yamusi gneissic granodiorite is relatively weak, and researchers are more focused on other rock masses in this area, and so much additional work is needed. We conducted geological, petrological, zircon U-Pb chronological, and geochemical analyses to investigate the petrogenesis and tectonic setting of this granodiorite and to provide new evidence for the northward subduction and accretion of the early Paleozoic Proto-Tethyan Ocean in the eastern part of the Qilian orogenic belt.

2. Regional Geological Background

The Qilian orogenic belt is an important part of the Central China Orogenic System. It is bounded by the Alxa Block to the north, the Qaidam Block to the south, and the North China Craton to the east, and it is separated from the Tarim Block to the west by the Altyn Tagh strike-slip fault (Figure 1). The Qilian orogenic belt can be divided, from north to south, into the North Qilian orogenic belt, the Central Qilian block, the South Qilian tectonic belt, and the Northern Qaidam tectonic belt [28] (Figure 1). A continental rift zone [28] or accretionary mélange zone [37,38], which is known as the Lajishan tectonic zone, developed during the early Paleozoic period in the Riyueshan and Lajishan areas around Guanting, where the Central Qilian block and the South Qilian tectonic zone connect. The metamorphic basement of the Central Qilian block is similar to the metamorphic basement of the northern margin of the Qaidam Basin, the Qaidam and northern East Kunlun terranes, and the Yangtze Plate, which developed during the formation of Rodinia (1000–900 Ma) [39]. The formation of the Qilian orogenic belt is the result of the convergence and collision of the Alxa Block and the Qilian and Qaidam–Eastern Kunlun massifs during the early Paleozoic period [40].

The study area is located at the intersection of the northern margin of the West Qinling tectonic zone, the Hualong micro-massif, and the Lajishan tectonic zone, and it has a complex compositional and tectonic history (Figure 2). The northern edge of the West Qinling tectonic zone comprises the widespread Lower Triassic Longwuhe Formation and is intruded by numerous Indosinian granites. The Hualong micro-massif contains the Paleoproterozoic Hualong Group and Cenozoic strata, and early Paleozoic composite plutons are found in the Hualong Group [32,41,42]. The main body of the Hualong group in the research area is a set of plagioclase hornblende schists with a small amount of gneiss combinations. Recent zircon U-Pb ages suggest that the protoliths of the Hualong Group most likely formed during the Neoproterozoic period rather than the Paleoproterozoic period, and they record the rifting of Rodinia [38,43–45]. The Lajishan tectonic belt extends approximately east–west over >200 km in the Qilian Orogen with a width of 10–30 km, and it is bounded by fractures on both sides. A Precambrian metamorphic complex developed on the northern and southern sides of the Lajishan tectonic belt, and early Paleozoic volcanic strata and Caledonian quartz diorites and granodiorites were emplaced and late Silurian–early Devonian sedimentary strata were deposited in the interior of the belt. Some researchers have interpreted that the Lajishan tectonic belt was a part of a complex tectonic mélange belt formed by the northward subduction and accretion of the Proto-Tethyan Ocean [38,46].

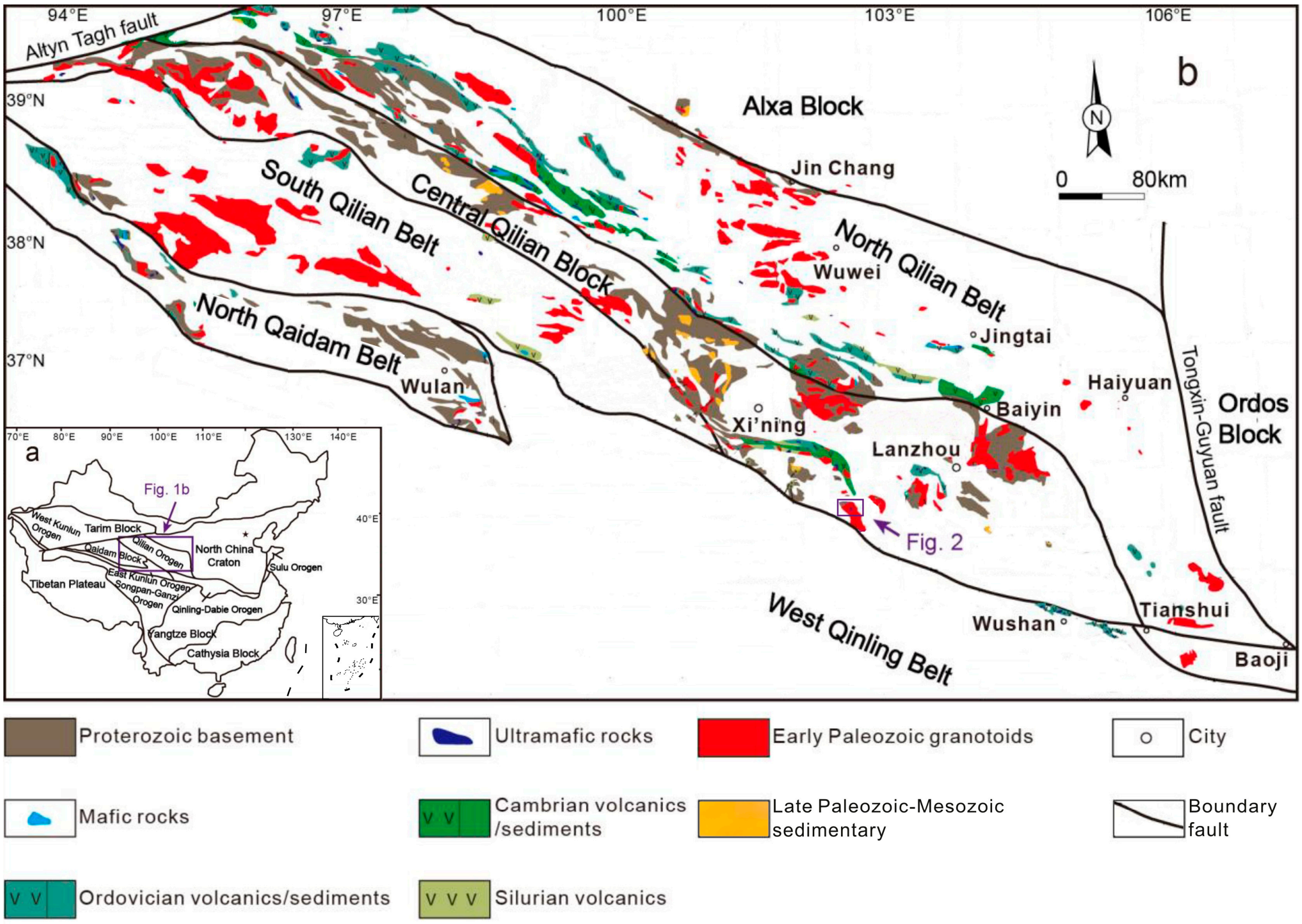

Figure 1. (**a**) Geological sketch map showing the major tectonic units of China (modified after [47]). (**b**) Simplified geological map of the Qilian orogenic belt showing the distribution of the Precambrian basement and the early Paleozoic volcanics, granitoids, and mafic and ultramafic rocks (modified after [35,48]).

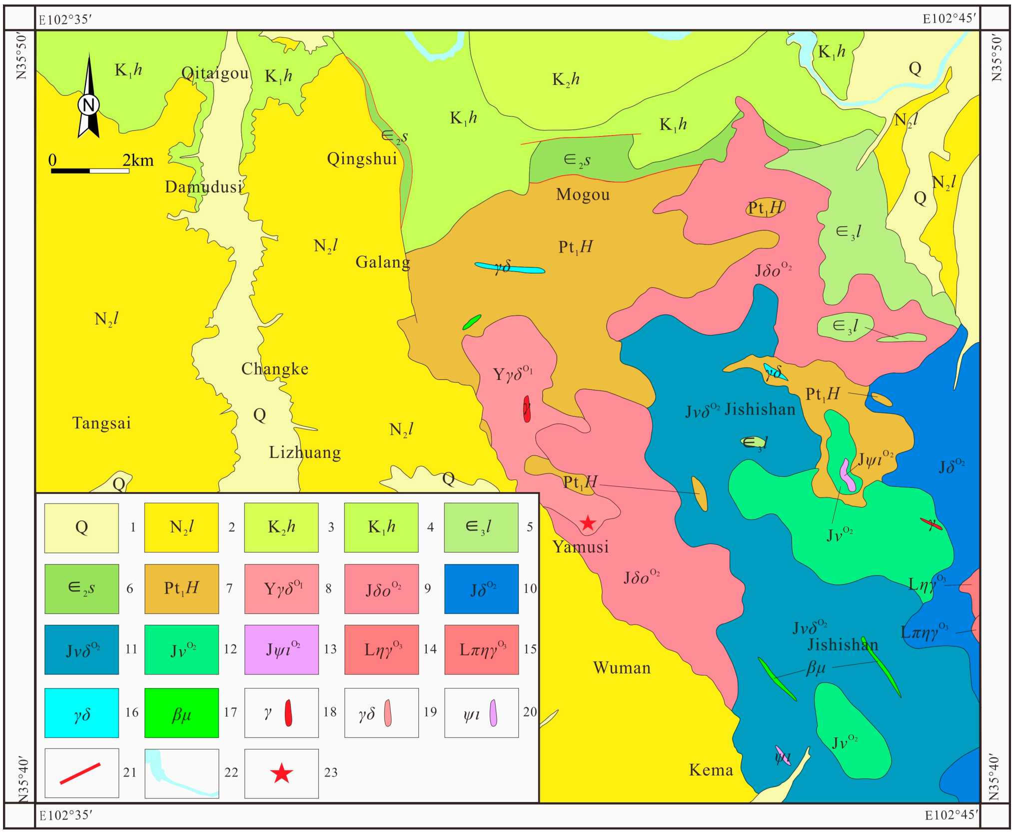

Figure 2. Simplified geological map of the study area. Legend explanation: 1—Quaternary; 2—Neogene Linxia Formation; 3—Late Cretaceous Hekou Formation II; 4—Early Cretaceous Hekou Formation I; 5—Late Cambrian Liudogou Formation; 6—Middle Cambrian Shengou Formation; 7—Paleoproterozoic Hualong Group; 8—Early Ordovician Yamusi granodiorite; 9—Middle Ordovician Jishishan quartz diorite; 10—Middle Ordovician Jishishan diorite; 11—Middle Ordovician Jishishan gabbro-diorite; 12—Middle Ordovician Jishishan gabbro; 13—Middle Ordovician Jishishang pyroxenite; 14—Late Ordovician Leijishan monzonite granite; 15—Late Ordovician Leijishan porphyritic monzonite granite; 16—granodiorite; 17—diabase; 18—granitic vein; 19—granodioritic vein; 20—gabbro veins; 21—faults; 22—river; and 23—sampling locations.

3. Geological and Lithological Characteristics of the Yamusi Granodiorite

The Yamusi granodiorite is located in the Hualong micro-massifs in the South Qilian Orogen in Xunhua County, Qinghai Province. The granodiorite is exposed over ~7.8 km^2 and exhibits a gneissic foliation ranging from 82°∠37° to 90°∠40°. The northern margin of the granodiorite intrudes on the Paleoproterozoic Hualong Group, the eastern margin is intruded upon by the Jishishan mafic–intermediate complex, and the western boundary is in angular unconformity with the Cenozoic Linxia Formation (Figures 1 and 2).

The Yamusi granodiorite is gray with a gneissic texture and consists mainly of plagioclase (45%–50%), quartz (25%–30%), K-feldspar (5%–10%), amphibole (~5%), and biotite (~5%). Plagioclase is pale gray, euhedral to subhedral, prismatic, and has polysynthetic twins. Amphibole crystals are typically lamellar, euhedral, and yellowish-green under plane-polarized light, with visible chlorite. Biotite crystals are primarily prismatic or acicular, with gray–brown parallel extinctions under plane-polarized light. Quartz crystals are primarily anhedral, and undulose extinction is observed in some crystals (Figure 3). The formation of the gneissic foliation of the Yamusi granodiorite is related to both its mineral composition and its crystallization, as well as its tectonic environment of northward subduction.

Figure 3. Field photograph and microphotographs of Yamusi granodiorite: (**a**) field photograph of Yamusi granodiorite; (**b**–**d**) microphotographs of Yamusi granodiorite. Abbreviations: Hb, amphiboles; Bi, biotite; Pl, plagioclase; and Q, quartz.

4. Measurement Methods

Sample PM611-3-1 was collected from Yamusi in Xunhua County, Qinghai Province (35°43′36″ N, 102°38′35″ E). The rock sample was crushed to 0.180–0.154 mm and zircon grains were separated using conventional magnetic and heavy liquid methods, and then the grains with better crystal shapes and good transparency were selected for analysis. The zircon grains were first placed on double-sided tape and then fixed with colorless and transparent epoxy resin. After the epoxy resin was fully cured, the surface was polished until the interiors of the grains were exposed. Optical microphotographs and cathodoluminescence (CL) images were taken of the grains, and they were analyzed using laser ablation inductively coupled plasma mass spectrometry (LA–ICP–MS).

The CL Imaging employed a scanning electron microscope fitted with a CL instrument at the Beijing GeoAnalysis Company (Beijing, China) to visualize the zircon's morphology and internal structures, and in situ U-Pb isotope analyses of individual zircon grains were performed using an ELAN 6100 DRC quadrupole mass spectrometer attached to a GeoLas 200M 193 nm ArF excimer laser ablation system at the State Key Laboratory of Continental Dynamics, Northwest University, using standard procedures. The analysis spots were selected to avoid internal fractures, inclusions, and areas with different geneses to obtain accurate ages. The analyses involved a beam diameter of 30 μm and ablation to a depth of 20–40 μm. Isotopic compositions were determined using zircon 91500 as the external standard, and the element contents were determined using NIST SRM 610 as the external standard and ^{29}Si as the internal standard. The detailed analytical procedures and instrument parameters have been described previously [49]. The isotopic ratios and element contents were processed using GLITTER version 4.0 [50], and common Pb was corrected using the method of Andersen. Zircon age calculations and U-Pb concordia diagrams were produced using Isoplot version 2.49 [51].

Whole-rock major element analyses were carried out by X-ray florescence spectrometry (XRF) at the Key Laboratory of Western Mineral Resource and Geological Engineering of the Ministry of Education. The analyses included two major steps: (1) Calculation of the loss on ignition (LOI), where the crucible was dried in an oven at 150 °C for 3 h and then weighed (W1). Approximately 1 g of sample was then added to the crucible, weighed (W2), and placed in a muffle furnace at 900 °C for 8 h, after which it was cooled and placed in a desiccator for 20 min and weighed again (W3). The LOI was then calculated using the formula LOI = (W1 + W2 − W3)/W2. (2) Glass fusion of the sample was used to determine the major element compositions, where 0.50 g of sample was weighed, anhydrous lithium tetraborate and ammonium nitrate were added as oxidants, and the mixture was placed in a platinum crucible with an appropriate amount of lithium bromide and heated to ~1200 °C to produce glass flakes. The composition was then measured using an XRF spectrometer.

The whole-rock rare earth and trace-element analyses were carried out at the Key Laboratory of Western Mineral Resource and Geological Engineering of the Ministry of Education using a Thermo X7 ICP–MS, with an analytical precision and accuracy of <10%. The samples were ground to <200 mesh, and 500 mg was placed in a PTFE crucible. Then, 1.0 mL of high purity HF and 1.5 mL of high purity HNO_3 were repeatedly added, heated, and cooled according to standard procedures. The samples were finally diluted to 50 mL in a centrifuge tube, and the solution was analyzed by ICP–MS.

5. Results

5.1. Zircon U-Pb Age

Most of the zircon grains in the Yamusi granodiorite (sample No. PM611-3-1) were colorless and transparent-to-pale-yellow, with short or long euhedral prisms, and they were generally 120–250 μm long and 50–120 μm wide, with aspect ratios of 1:1–1:3. The CL images showed that most grains had typical magmatic concentric zoning (Figure 4), and the grains all had Th/U ratios of >0.1, indicating a magmatic origin [52]. Twenty-five spots were analyzed, and they all produced valid results. The analyses plot on the concordia line indicated good concordance, suggesting that the zircons remained a closed system for the U-Pb, with little loss of Pb [53,54]. The analyses yielded $^{206}Pb/^{238}U$ ages of 484–476 Ma, with a weighted mean of 480.3 ± 1.3 Ma (MSWD = 0.21; Figure 5), which represents the magmatic crystallization age of the Yamusi granodiorite (Table 1). Therefore, we proposed that the intrusion age of the granodiorite was 480 Ma, during the early Ordovician period.

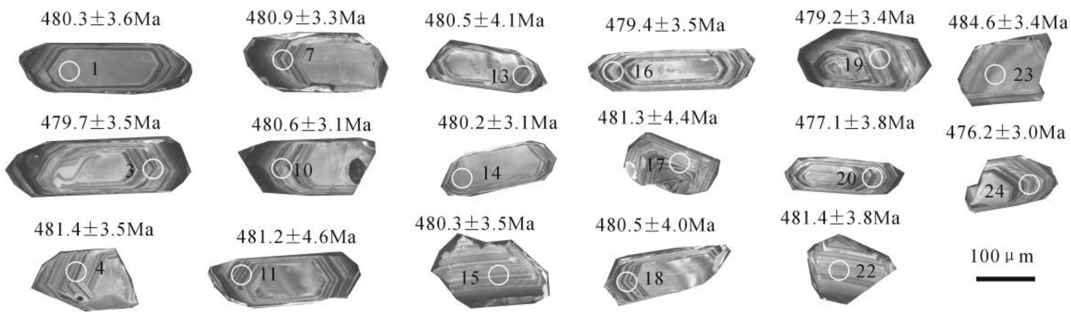

Figure 4. CL images and ages of the representative zircon grains from the Yamusi granodiorite.

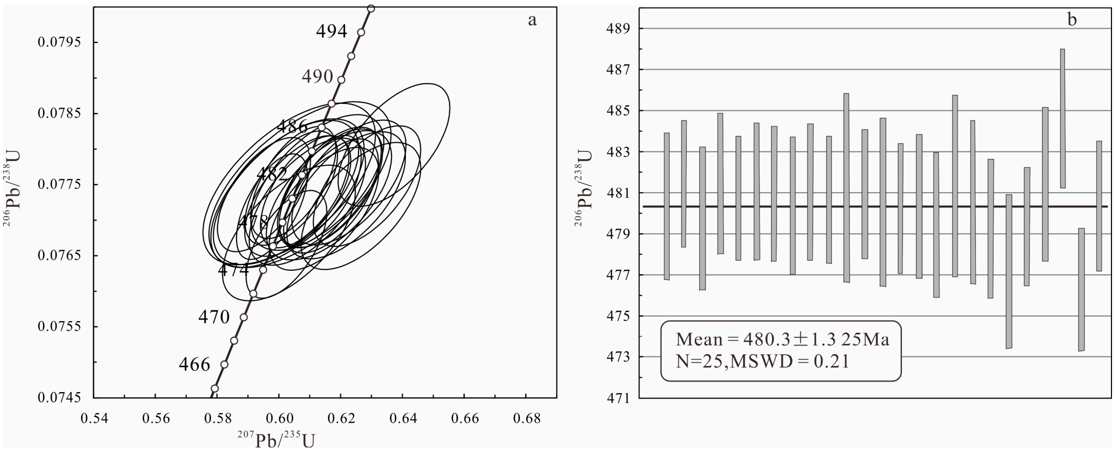

Figure 5. Zircon U-Pb concordia diagram (**a**) and average age (**b**) of the Yamusi granodiorite.

5.2. Geochemistry Characteristics

A total of 11 samples were selected for geochemical analysis, and the results are listed in Table 2. The samples had high SiO_2 (60.0–63.0 wt.%, mean = 61.9 wt.%) and Al_2O_3 contents (17.6–18.7 wt.%, mean = 18.1 wt.%), low MgO contents (1.5–2.26 wt.%, mean = 1.75 wt.%), TiO_2 contents of 0.33–0.44 wt.% (mean = 0.40 wt.%), and low LOI values (<2%). All samples were plotted in a granodiorite field on a QAP diagram (Figure 6a) and in a calc-alkaline field on an AFM diagram (Figure 6b). The samples yielded Al saturation index (A/CNK) values of 0.91–1.02 (mean = 0.99), indicating that they were metaluminous–weakly peraluminous (Figure 6b). The samples yielded differentiation index (DI) values of 57.6–63.1 (mean = 59.3) and Rittman index values of 0.96–1.26 (mean = 1.21), indicating that they were calc-alkaline. The samples had CaO contents of 5.47–6.67 wt.% (mean = 6.24 wt.%), Na_2O contents of 2.83–3.83 wt.% (mean = 3.05 wt.%), and K_2O contents of 1.29–2.13 wt.% (mean = 1.73 wt.%), indicating that they belonged to the medium K calc–alkaline series (Figure 7a). In addition, the geochemical analysis showed that these batches were magnesian granites [55], which are generally considered oxidized arc systems.

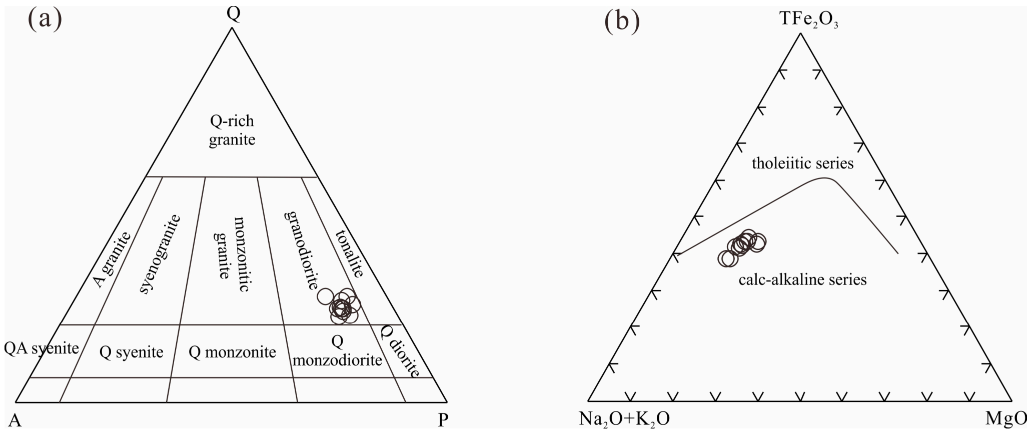

Figure 6. QAP diagram (**a**) and AFM diagram (**b**) of the Yamusi granodiorite.

Table 1. LA-ICP-MS U-Pb isotopic compositions of the zircon grains from the Yamusi granodiorite (PM611-3-1).

Point Number	Pb	Th	U	Th/U	$^{206}Pb/^{238}U$		$^{207}Pb/^{235}U$		$^{207}Pb/^{206}Pb$		$^{208}Pb/^{232}Th$		$^{206}Pb/^{238}U$		$^{207}Pb/^{235}U$		$^{207}Pb/^{206}Pb$	
	($\times10^{-6}$)				Ratio	1σ	Ratio	1σ	Ratio	1σ	Ratio	1σ	Age (Ma)	1σ	Age (Ma)	1σ	Age (Ma)	1σ
1	14.0	52.9	146.5	0.36	0.0774	0.0006	0.6162	0.0134	0.0578	0.0014	0.0237	0.0004	480	4	488	8	521	51
2	27.2	86.4	288.7	0.30	0.0775	0.0005	0.6047	0.0091	0.0566	0.0010	0.0241	0.0003	481	3	480	6	474	39
3	55.8	433.3	516.5	0.84	0.0773	0.0006	0.6092	0.0124	0.0572	0.0013	0.0238	0.0003	480	4	483	8	498	49
4	17.2	68.7	178.1	0.39	0.0775	0.0006	0.6227	0.0122	0.0583	0.0013	0.0236	0.0003	481	3	492	8	539	47
5	33.6	132.6	346.4	0.38	0.0774	0.0005	0.6134	0.0088	0.0575	0.0010	0.0249	0.0003	481	3	486	6	509	37
6	21.5	93.7	217.4	0.43	0.0775	0.0006	0.6286	0.0115	0.0588	0.0012	0.0253	0.0003	481	3	495	7	561	44
7	22.1	91.6	224.9	0.41	0.0775	0.0006	0.6168	0.0111	0.0578	0.0012	0.0253	0.0003	481	3	488	7	521	44
8	21.0	71.5	219.8	0.33	0.0773	0.0006	0.6062	0.0113	0.0568	0.0012	0.0244	0.0004	480	3	481	7	485	46
9	41.4	234.9	397.3	0.59	0.0775	0.0006	0.6164	0.0111	0.0577	0.0012	0.0261	0.0003	481	3	488	7	519	44
10	29.7	142.8	298.0	0.48	0.0774	0.0005	0.6084	0.0094	0.0570	0.0010	0.0238	0.0002	481	3	483	6	491	39
11	21.1	82.3	216.4	0.38	0.0775	0.0008	0.6069	0.0195	0.0568	0.0019	0.0246	0.0006	481	5	482	12	483	74
12	32.4	202.4	311.5	0.65	0.0775	0.0005	0.6041	0.0099	0.0566	0.0011	0.0234	0.0002	481	3	480	6	474	41
13	25.0	176.1	236.7	0.74	0.0774	0.0007	0.6028	0.0164	0.0565	0.0016	0.0215	0.0003	481	4	479	10	471	63
14	26.1	124.7	257.8	0.48	0.0773	0.0005	0.6169	0.0101	0.0579	0.0011	0.0248	0.0003	480	3	488	6	524	41
15	14.3	49.6	147.9	0.34	0.0774	0.0006	0.6218	0.0127	0.0583	0.0013	0.0246	0.0004	480	4	491	8	540	49
16	34.1	200.9	327.9	0.61	0.0772	0.0006	0.6266	0.0128	0.0589	0.0013	0.0235	0.0003	479	4	494	8	562	48
17	16.4	57.6	168.2	0.34	0.0775	0.0008	0.6034	0.0184	0.0565	0.0018	0.0246	0.0006	481	4	479	12	470	70
18	27.9	124.6	278.3	0.45	0.0774	0.0007	0.6023	0.0155	0.0565	0.0016	0.0242	0.0004	481	4	479	10	469	60
19	29.0	123.2	291.2	0.42	0.0772	0.0006	0.6146	0.0117	0.0578	0.0012	0.0243	0.0003	479	3	487	7	521	46
20	45.6	327.1	416.6	0.79	0.0768	0.0006	0.6033	0.0142	0.0570	0.0015	0.0244	0.0003	477	4	479	9	489	56
21	56.3	327.4	535.8	0.61	0.0772	0.0005	0.5978	0.0076	0.0562	0.0009	0.0246	0.0002	479	3	476	5	459	33
22	14.3	49.8	146.3	0.34	0.0775	0.0006	0.6125	0.0142	0.0573	0.0014	0.0243	0.0004	481	4	485	9	502	55
23	16.1	62.9	160.5	0.39	0.0781	0.0006	0.6373	0.0120	0.0592	0.0012	0.0244	0.0003	485	3	501	7	575	45
24	64.3	432.5	600.1	0.72	0.0767	0.0005	0.6025	0.0086	0.0570	0.0010	0.0234	0.0002	476	3	479	5	491	37
25	27.4	87.9	283.0	0.31	0.0774	0.0005	0.5952	0.0099	0.0558	0.0011	0.0234	0.0003	480	3	474	6	444	41

Table 2. Major (%) and trace ($\times 10^{-6}$) element analyses of the Yamusi granodiorite.

Sample No.	PM611/2DH$_2$	PM611/3DH$_1$	PM611/3DH$_2$	PM611/5DH$_1$	PM611/5DH$_2$	PM611/5DH$_3$	PM611/5DH$_4$	PM611/5DH$_5$	PM611/5DH$_6$	D4369/DH$_1$	D6331/DH$_1$
SiO_2	62.24	62.67	61.51	62.37	61.91	60.30	62.40	62.02	62.95	62.09	60.93
TiO_2	0.33	0.38	0.49	0.44	0.40	0.42	0.35	0.44	0.40	0.35	0.44
Al_2O_3	17.68	17.58	18.14	18.31	18.00	18.20	18.43	18.53	17.60	17.88	18.72
TFe_2O_3	5.35	4.37	5.34	4.64	4.73	4.86	4.54	4.64	4.12	4.95	4.65
MnO	0.14	0.14	0.18	0.16	0.16	0.16	0.15	0.17	0.16	0.13	0.15
MgO	2.26	1.53	1.98	1.59	1.67	1.73	1.52	1.68	1.50	2.13	1.69
CaO	6.35	6.15	6.67	6.27	6.28	6.43	6.43	6.15	5.47	6.15	6.37
Na_2O	2.83	3.83	3.04	2.98	2.88	2.97	2.97	3.05	2.88	3.23	2.96
K_2O	1.90	1.63	2.01	1.68	1.39	1.70	1.83	1.85	2.13	1.29	1.70
P_2O_5	0.13	0.21	0.23	0.24	0.22	0.22	0.20	0.22	0.20	0.16	0.24
LOI	1.04	0.99	1.38	0.88	1.63	1.11	0.86	1.13	1.40	1.13	1.20
TOTAL	100.25	99.48	100.97	99.56	99.27	98.10	99.68	99.88	98.81	99.49	99.05
A/CNK	0.97	0.91	0.94	1.01	1.02	0.99	0.99	1.02	1.04	1.00	1.02
A/NK	2.63	2.18	2.53	2.72	2.88	2.71	2.68	2.64	2.50	2.66	2.79
La	9.27	3.87	17.32	6.51	3.34	4.38	4.59	9.86	6.79	12.18	8.72
Ce	16.35	8.42	36.80	15.35	8.45	10.13	10.17	21.01	14.50	22.83	18.39
Pr	1.77	1.08	3.84	1.83	1.11	1.36	1.40	2.62	1.82	2.49	2.43
Nd	6.86	5.03	14.66	7.96	5.29	6.40	6.62	10.96	8.21	10.09	10.40
Sm	1.50	1.35	2.51	1.87	1.52	1.77	1.75	2.43	1.97	2.03	2.32
Eu	0.61	0.60	0.87	0.74	0.69	0.75	0.87	1.03	0.96	0.87	1.02
Gd	1.90	1.70	2.48	2.06	1.81	2.10	2.10	2.74	2.31	2.24	2.58
Tb	0.26	0.25	0.35	0.32	0.28	0.30	0.34	0.39	0.34	0.31	0.39
Dy	1.64	1.61	2.02	1.89	1.80	2.04	2.03	2.50	2.10	1.84	2.46
Ho	0.33	0.35	0.39	0.42	0.37	0.42	0.43	0.51	0.43	0.37	0.50
Er	1.08	1.01	1.26	1.23	1.17	1.27	1.37	1.57	1.31	1.12	1.51
Tm	0.16	0.17	0.19	0.18	0.18	0.19	0.21	0.24	0.20	0.17	0.22
Yb	1.18	1.19	1.29	1.34	1.28	1.45	1.58	1.69	1.50	1.24	1.66
Lu	0.18	0.18	0.20	0.22	0.19	0.22	0.24	0.29	0.22	0.19	0.26
$(La/Yb)_N$	5.31	2.20	9.03	3.29	1.77	2.03	1.96	3.94	3.05	6.63	3.55
δEu	1.10	1.21	1.05	1.15	1.27	1.19	1.38	1.22	1.38	1.24	1.27
Li	8.05	7.89	10.18	4.69	7.74	5.51	24.46	18.10	19.35	12.35	19.19
Be	0.59	0.85	0.87	0.95	0.91	0.85	0.87	0.90	0.89	0.79	0.93
Sc	11.35	3.89	4.93	4.15	4.04	4.58	6.87	6.45	5.52	11.07	5.82
V	98.04	62.28	73.77	63.31	69.01	73.71	72.12	63.38	55.50	87.65	66.73
Cr	12.00	1.08	1.31	1.18	1.40	1.23	1.61	1.13	1.36	14.17	1.23
Co	11.47	7.34	9.09	7.02	7.88	8.72	7.53	6.79	6.22	10.29	6.95

Table 2. *Cont.*

Sample No.	PM611/2DH$_2$	PM611/3DH$_1$	PM611/3DH$_2$	PM611/5DH$_1$	PM611/5DH$_2$	PM611/5DH$_3$	PM611/5DH$_4$	PM611/5DH$_5$	PM611/5DH$_6$	D4369/DH$_1$	D6331/DH$_1$
Ni	6.26	2.83	3.30	2.91	3.00	3.26	2.69	2.90	2.81	7.48	2.82
Cu	4.34	5.91	8.07	4.36	8.65	17.29	7.97	2.00	1.26	3.30	4.35
Zn	53.56	59.08	74.53	65.69	64.25	68.29	64.91	74.69	69.60	61.45	68.37
Ga	13.11	14.10	15.65	14.87	13.96	14.84	17.68	18.77	17.68	16.49	18.92
Rb	52.20	55.54	63.51	60.59	48.74	57.20	74.12	79.77	89.28	38.06	65.81
Sr	328	438	442	603	421	442	534	564	501.00	544	529
Y	9.32	9.39	11.14	11.21	10.50	11.50	12.22	13.78	12.27	10.30	13.64
Zr	35.71	47.18	55.45	59.35	51.30	59.63	50.63	66.57	48.00	65.35	65.76
Nb	4.06	6.77	8.68	7.59	7.08	7.93	6.77	9.06	8.63	4.18	8.89
Mo	0.08	0.07	0.10	0.27	0.21	0.48	0.04	0.05	0.07	0.03	0.02
Cd	0.09	0.11	0.10	0.08	0.09	0.13	0.10	0.08	0.07	0.13	0.08
In	0.03	0.02	0.03	0.03	0.03	0.03	0.03	0.03	0.03	0.03	0.04
Cs	7.78	7.11	9.99	9.20	8.25	11.88	13.35	11.22	12.68	2.28	8.20
Ba	871	398	626	446	423.00	673	607	640	721	557	658
Hf	1.25	1.50	1.68	1.84	1.59	1.87	1.68	2.14	1.48	1.87	1.99
Ta	0.29	0.36	0.51	0.41	0.41	0.52	0.57	0.67	0.58	0.26	0.52
Pb	11.03	6.31	6.63	6.37	6.08	7.19	8.06	7.83	7.45	10.14	6.35
Bi	0.03	0.01	0.01	0.04	0.03	0.04	0.04	0.01	0.01	0.01	0.01
Th	4.28	0.87	3.86	1.86	0.76	0.90	1.08	2.16	1.41	3.53	1.97
U	0.68	0.51	0.57	0.43	0.37	0.48	0.55	0.53	0.31	0.45	0.32

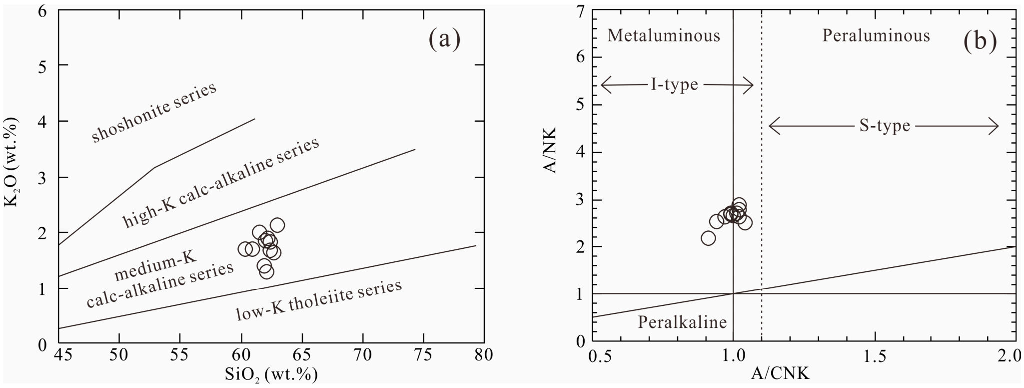

Figure 7. SiO_2 vs. K_2O diagram (**a**) and A/NK vs. A/CNK diagram (**b**) of the Yamusi granodiorite [56]. The dotted line represents the boundary between the I- and S-type granites [57].

On chondrite-normalized rare earth element (REE) diagrams (Figure 8a), the samples showed fractionation between the light and heavy REEs ($(La/Yb)_N$ = 1.76–9.0, mean = 3.88), enrichment in the light REEs ($(La/Dy)_N$ = 1.93–8.92, mean = 4.12), and no significant fractionation between the medium and heavy REEs ($(Gd/Yb)_N$ = 1.07–1.54, mean = 1.26). The REE patterns generally dipped smoothly to the right, which was consistent with the REE partitioning curves of dacite [58–64]. The samples yielded δEu values of 1.04–1.38, with slightly positive Eu anomalies, indicating that the plagioclase did not undergo significant crystal fractionation.

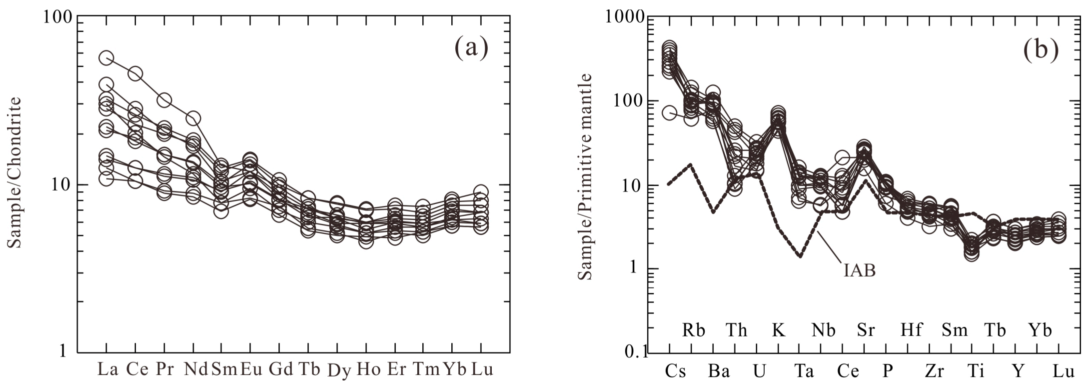

Figure 8. Chondrite-normalized REE patterns (**a**) and primitive mantle-normalized trace element patterns (**b**) of the Yamusi granodiorite. The chondrite values were obtained from reference [64] and the primitive mantle values were obtained from reference [65].

The samples had high Sr (328–603 ppm, mean = 486 ppm), Cs (2.28–13.3 ppm, mean = 9.26 ppm), and Ba (398–871 ppm, mean = 602 ppm) contents and low Y (9.32–13.6 ppm, mean = 602 ppm), Yb (1.17–1.68 ppm, mean = 1.40 ppm), Nb (4.06–9.06 ppm, mean = 7.24 ppm), and Ta (0.25–0.67 ppm, mean = 0.46 ppm) contents (Table 2), with Nb/Ta ratios of 11.9–18.8 (mean = 159) and Sr/Y ratios of 35.2–53.8 (mean = 42.1). On the NMORB-normalized incompatible element spider diagram (Figure 8b), the samples were enriched in large-ion lithophile elements (LILEs; e.g., Cs, Rb, and Ba) and depleted in high-field-strength elements (HFSEs; e.g., Nb, Ta, and Ti; Figure 8b), similar to the incompatible element patterns of adakitic granites and arc magmatic rocks.

6. Discussion

6.1. Rock Type

Yamusi granodiorite is composed mainly of quartz, plagioclase, biotite, and amphibole, and it is a quasi-aluminous–weakly peraluminous medium K–Ca–alkaline rock

(Figure 7b). It is characterized by high SiO_2 contents (60.3–63.0 wt.%), is Na-rich and K-poor (K_2O/Na_2O = 0.40–0.73), Al-rich (Al_2O_3 > 15 wt.%), and has low Mg# (39.9–46.0, mean = 42.1) and MgO (1.5–2.26 wt.%, mean = 1.75 wt.%) contents. Its REE patterns showed enrichment in LREEs and depletion in HREEs, with little variation from Gd to Lu and a slight upward shift in the REE distribution curve toward the HREEs (Figure 8a), indicating residual amphibole in the magma source [54,58]. The samples had weak positive Eu anomalies (δEu = 1.05–1.38; Figure 8a), high Ba contents and Sr/Y ratios, and low Y and Yb contents, with enrichment in large-ion lithophile elements (Cs, Rb, and Ba) and depletion in high-field-strength elements (Nb, Ta, Zr, Hf, and Ti; Figure 8b). The Yamusi granodiorite was plotted in the adakites field (Figure 9). Figure 9 shows that the adakite plots for the Yamusi granodiorite were predominantly within the defined adakite field, with no plot falling in the overlapping region of the adakite and island arc domains. This may indicate that the sample satisfied the geochemical constraints, and the rocks could be classified as adakites [66].

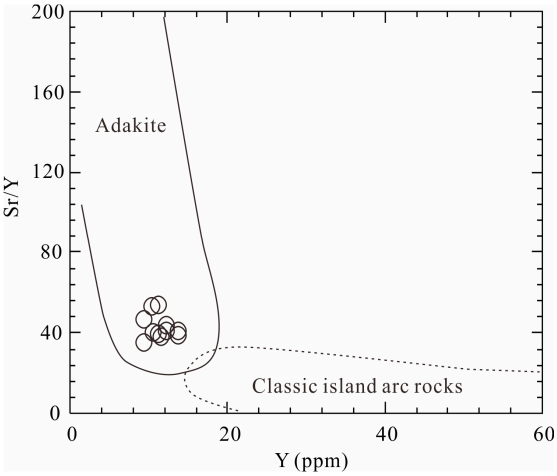

Figure 9. Sr/Y vs. Y diagram [61] for the Yamusi granodiorite.

Adakites typically have the following geochemical characteristics: $SiO_2 \geq 56$ wt.%; $Al_2O_3 \geq 15$ wt.%; MgO < 6 wt.%; low K_2O/Na_2O ratios (<0.5); $Mg^{\#}$ ($Mg^{2+}/(Mg^{2+} + Fe^{total})$) values of >0.47 and even up to 0.70; high Sr contents (400–2000 ppm); low Y and HREE contents (Y $\leq$ 18 ppm and Yb $\leq$ 1.9 ppm, respectively); and strongly fractionated REE patterns. Thus, adakites have high La/Yb and Sr/Y ratios, depletion in HFSEs, positive or no Sr and Eu anomalies, and similar isotopic compositions to MORB ($^{144}Nd/^{143}Nd$ > 0.51 and $^{87}Sr/^{86}Sr$ < 0.71, respectively) [67]. The Yamusi granodiorite had high SiO_2 and Al_2O_3 and low MgO contents, enrichment in LREEs, limited fractionation between the middle and heavy REEs, and slightly positive Eu anomalies, all of which were similar to the geochemical characteristics of adakites.

6.2. Petrogenesis and Magma Source

Various mechanisms have been proposed for the formation of adakites, including: (1) the partial melting of subducted oceanic crust [57–62,68,69]; (2) the partial melting of thickened subcrustal material [70–72]; (3) partial subducted subcrustal melting [70,73–75]; and (4) the fractional crystallization of basaltic magma [76]. The Yamusi granodiorite had low MgO (1.5–2.26 wt.%), TFe_2O_3 (4.12–5.35 wt.%), Cr (mean = 3.43 ppm), Co (mean = 8.12 ppm), V (mean = 71.4 ppm), and Ni (mean = 3.66 ppm) contents, suggesting that it may have been derived from the continental crust. The Nb/U (mean = 16.6) and Ta/U (mean = 1.05) ratios of the granodiorite were lower than the corresponding MORB and OIB ratios (Nb/U ≈ 47 and Ta/U ≈ 2.7) [63] and were closer to the crustal ratios (Nb/U ≈ 12.1 and Ta/U ≈ 1.1) [67], which was again consistent with a crustal origin. On a discrimination diagram (Figure 10), most samples were plotted in the lower crustal amphibolite melt field, which suggests that the source of the granodiorite may have been dominated by lower crustal metabasic rocks [77,78]. Moreover, the sample was metaluminous–weakly peraluminous and had high La/Yb and low Yb contents, which may suggest that its crustal source area was basaltic rocks, with a high degree of residual garnet or hornblende.

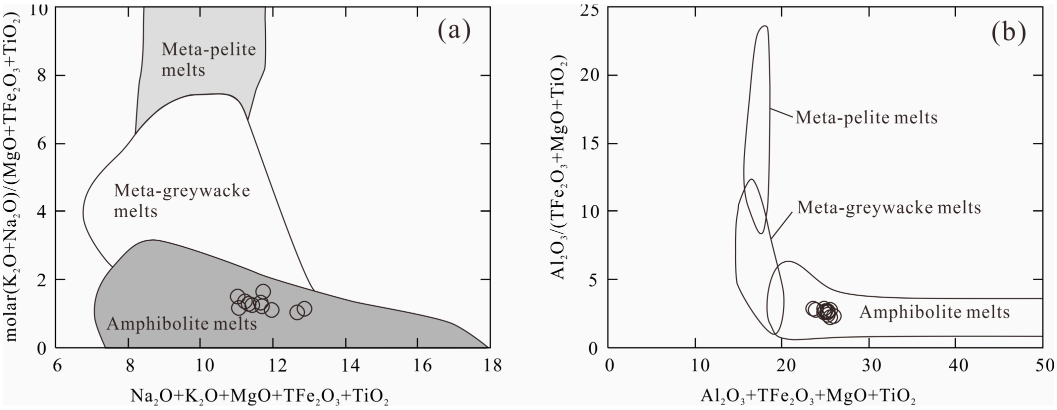

Figure 10. Chemical content contrasts for the experimental melt between the Yamusi granodiorite and meta-mudstone-, greywacke-, meta-amphibolite-derived samples [79,80]. (**a**) Na_2O + K_2O + MgO + TFe_2O_3 + TiO_2 vs. molar (K_2O + Na_2O)/(MgO + TFe_2O_3 + TiO_2) diagram. (**b**) Al_2O_3 + TFe_2O_3 + MgO + TiO_2 vs. Al_2O_3/(TFe_2O_3 + MgO + TiO_2) diagram of the Yamusi granodiorite.

Experimental petrological studies have shown that the Mg# value of adakites formed by the partial melting of a basaltic source at 1–4 GPa is <50, but when the slab melt is mixed with mantle wedge peridotite, its Mg# value increases rapidly to >50 [81]. The Mg# value of granite is an important basis for determining whether it is a crust-mantle-mixed source or of lower crustal origin. The Nb/Ta ratios of the Yamusi granodiorite were 11.9–18.8 (mean = 15.9) and its Mg# values were 39.9–46.0 (mean = 42.1), and along with the trace element characteristics of the samples, this suggests that the magma that formed the granodiorite may have undergone some degree of mantle-mixing. It may also suggest that the sample may not have been of pure crust or mantle origin. The low differentiation index of the granodiorite (DI = 57.6–59.5, mean = 59.3) implied weak fractional crystallization during magmatic evolution. On the chondrite-normalized REE diagram (Figure 8), there was clear fractionation between the light and heavy REEs ($(La/Yb)_N$ = 1.77–9.03, mean = 3.88), and there was limited fractionation between the medium and heavy REEs ($(Gd/Yb)_N$ = 1.07–1.54, mean = 1.26), indicating the presence of residual amphibole in the magma source [82]. The weak positive Eu anomalies (δEu = 1.04–1.38, mean = 1.22) and high Sr contents (328–603 ppm, mean = 486 ppm) implied little residual plagioclase in the magma source and little fractional crystallization of the plagioclase during the magmatic evolution [79,80]. Early Paleozoic volcanic strata, ophiolite suite, Caledonian quartz diorites, and granodiorites have developed in the Lajishan tectonic belt near the study area [38,46]. Many researchers have studied other rock masses near the study area and found that many rock masses have characteristics that derived from the partial melting of the mantle, with possible admixture of the crustal material [13,16,18,28,29,38,83,84]. These findings also provide evidence for this study. Therefore, the Yamusi granodiorite may have derived from the partial melting of the mantle in a subduction environment, which led to the formation of the parent magma. During the subsequent magmatic evolution, fractional crystallization would have been relatively limited.

6.3. Tectonic Environment and Geological Significance

The Yamusi granodiorite was characterized by enrichment in the light REEs and depletion in the heavy REEs, with enrichment in the LILEs (Cs, Rb, and Ba) and depletion in the HFSEs (Nb, Ta, and Ti) on a trace element spider diagram. These characteristics are consistent with those of arc magmas. On the tectonic discrimination diagrams (Figure 11), the samples were plotted in the volcanic arc fields; therefore, we proposed that the granodiorite was formed in a magmatic arc environment associated with the subduction of oceanic lithosphere. Therefore, it could also be inferred that the Yamusi granodiorite had properties similar to other post-collisional "adakitic" granitoid rocks in Tibet, many of which were derived during slab breakoff [85].

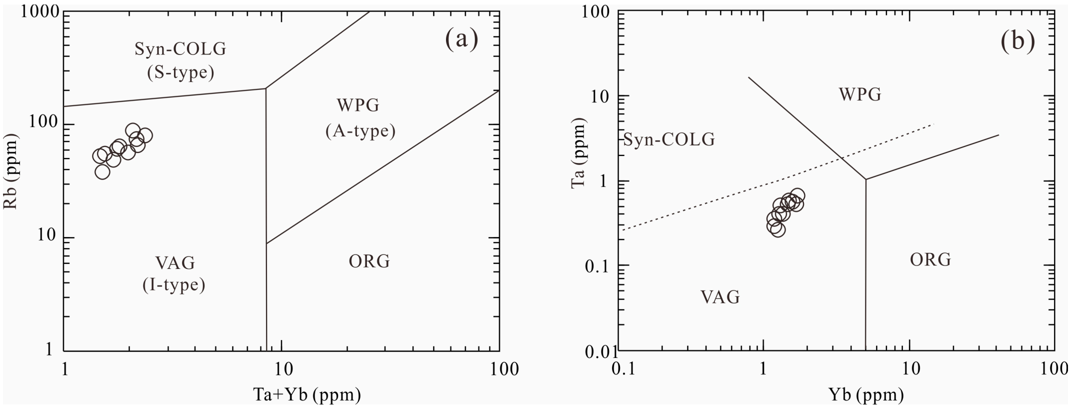

Figure 11. Rb vs. (Yb + Ta) diagram (**a**) and Yb vs. Ta diagram (**b**) for the Yamusi granodiorite [86–91]. Syn-COLG, syn-collisional granites; VAG, volcanic arc granite; WPG, within-plate granites; ORG, ocean ridge granites.

Previous studies [15,28,29] have suggested that there were at least two oceanic basin systems in the Qilian orogenic belt during the early Paleozoic period: the North Qilian Ocean between the Central Qilian and Alxa blocks and the Northern Qaidam Ocean (also known as the South Qilian Ocean) between the Qaidam and Central Qilian blocks. Both of these ocean basin systems are likely to be branches of the Proto-Tethyan oceanic domain located to the north of Gondwana [15,28,92]. The North Qilian Ocean began to subduct northward in the late early Cambrian period, forming a series of island arc and back-arc basin magmatic rocks during the early Cambrian–late Ordovician periods (520–445 Ma) [93]. The North Qilian Ocean is also thought to have been subducted to either the south or to both the south and north [94]. The South Qilian Ocean was also subducted northward beneath the Central Qilian block, and the early Paleozoic arc volcanic rocks of the Tanjianshan Group in the north of the HP–UHP metamorphic zone in the northern Qaidam Basin are the products of arc volcanism related to the northward subduction of an ocean on the northern margin of the Qaidam Basin [95]. Wu et al. [16,18] investigated the Aolaoshan granite (473 $\pm$ 15 Ma), the Saishitenshan granite (465.4 $\pm$ 3.5 Ma), and the Tuanyushan granodiorite (469.7 $\pm$ 4.6 Ma) on the northern margin of the Qaidam Basin and concluded that they formed in an island arc environment. Xia et al. [28] synthesized previous data from the gneisses, eclogites, and ultramafic rocks in the HP–UHP metamorphic zone in the northern Qaidam Basin–South Qilian tectonic belt and concluded that these rocks first underwent HP metamorphism below the stability field of coesite at 476–445 Ma and then underwent UHP metamorphism at 440–421 Ma. The early HP metamorphism is consistent with oceanic subduction, whereas the late ultrahigh-pressure metamorphism indicates continental subduction. Huang et al. [84] identified ophiolite mélange (441 Ma) in the Dadaoerji area on the southern margin of the Central Qilian block, which they proposed was a back-arc extensional setting caused by the northward subduction of the South Qilian oceanic crust. The mafic–ultramafic complexes (449–440 Ma) in the Hualong area on the southern margin of the Central Qilian block were formed at the end of the northward subduction and transitional collisional orogenic stage of the South Qilian Ocean [33]. The discovery of syn-collisional granites emplaced at 441 Ma in the Xitieshan area on the northern margin of the Qaidam Basin suggests that the Qaidam block collided with the

Central Qilian block [96] and that the northern Qaidam ocean closed, after which the Qilian orogenic belt entered an intra-continent tectonic evolutionary stage.

Based on the above data, the northward subduction of the northern Qaidam Ocean can be constrained to the middle Cambrian–early Silurian periods (520–440 Ma). The Yamusi granodiorite we studied is located in the eastern part of the South Qilian block and has an age of 480.3 ± 1.3 Ma. Geochemically, it is a metaluminous–weakly peraluminous calc-alkaline rock that is enriched in LILEs, including Ba and Th, and depleted in HFSEs (e.g., Nb, Ta, Zr, Hf, and Ti). The geochemical characteristics of the granodiorite are consistent with those of island arc magmatic rocks. Thus, on the basis of magmatic arc events associated with the northward subduction of the northern Qaidam Ocean, we suggest that the Yamusi granodiorite formed as a tectono-magmatic response to the arc magmatism caused by the northward subduction of the northern Qaidam Ocean beneath the Central Qilian orogenic belt during the early Paleozoic period.

7. Conclusions

1. The major element compositions and mineralogy of the Yamusi granodiorite indicate that it belongs to the metaluminous–weakly peraluminous, medium K calc–alkaline series. The crystallization age of the Yamusi granodiorite is 480.3 ± 1.3 Ma, indicating that the rock was formed during the early Ordovician period.
2. The Yamusi granodiorite is enriched in light rare earth elements and depleted in heavy rare earth elements. The trace element spider diagrams indicate that the granodiorite is enriched in large-ion lithophile elements, including Rb, Ba, and Th, and depleted in high-field-strength elements (Nb and Ta). These characteristics are typical of subduction-related arc magmatism.
3. The geochemical characteristics of the Yamusi granodiorite are similar to the geochemical characteristics of adakites. The Yamusi granodiorite represents a record of arc magmatism in the eastern part of the Qilian orogenic belt, beneath which the northern Qaidam ocean subducted northward during the early Paleozoic period.

Author Contributions: Conceptualization, X.P.; methodology, R.L.; software, Y.Z.; investigation, L.P., X.P., R.L., Z.L. and M.W.; resources, Y.C.; data curation, C.L.; writing—original draft preparation, L.P.; writing—review and editing, R.L. and Z.L.; supervision, R.L. and X.P.; funding acquisition, L.P. All authors have read and agreed to the published version of the manuscript.

Funding: This research was funded by the National Nature Sciences Foundation of China (grant numbers 42172236, 41872233, 41872235, and 41502191), the Natural Science Basic Research Plan in Shaanxi Province of China (grant numbers 2021JQ-241, 2019JM-312, 2019JQ-090, 2019JQ-209, and 2020JM-229, and 2020JQ-353), the Fundamental Research Funds for the Central Universities (grant numbers 300102270107, 300102270202, 300103183081, 300103120009, 300104282717, 300102279204, and 201810710233), the Commonweal Geological Survey, the Aluminum Corporation of China and the Land-Research Department of Qinghai Province (grant number 200801), and the Youth Innovation Team of Shaanxi Universities.

Acknowledgments: The authors would like to thank the Beijing Geoanalysis Ltd. (Beijing, China), the State Key Laboratory of Continental Dynamics (Northwest University, Xi'an, China). and the Key Laboratory of Western Mineral Resource and Geological Engineering of the Ministry of Education (Chang'an University, Xi'an, China) for their support and assistance with the zircon U-Pb and major and trace element analyses. The authors are grateful for the critical comments from the anonymous reviewers, which profoundly enhanced the quality of this manuscript.

Conflicts of Interest: The authors declare no conflict of interest.

References

1. Li, R.B.; Pei, X.Z.; Li, Z.C.; Patias, D.; Liu, C.J. Late Silurian to Early Devonian volcanics in the East Kunlun orogen, northern Tibetan Plateau: Record of postcollisional magmatism related to the evolution of the Proto-Tethys Ocean. *J. Geodyn.* **2020**, *140*, 101780. [CrossRef]
2. Li, R.B.; Pei, X.Z.; Wei, B.; Li, Z.C.; Pei, L.; Chen, G.C.; Chen, Y.X.; Liu, C.J. Middle Cambrian-Early Ordovician ophiolites in the central fault of the East Kunlun Orogen: Implications for an epicontinental setting related to Proto-Tethyan Ocean subduction. *Gondwana Res.* **2021**, *94*, 243–258. [CrossRef]
3. Pan, G.T.; Chen, Z.L.; Li, X.Z.; Yan, Y.J. *Formation and Evolution of East Tethys Geological Structure*; Geological Publishing House: Beijing, China, 1997; pp. 1–216.
4. Yin, H.F.; Zhang, K.X. Evolution and characteristics of central orogenic belt. *Earth Sci. J. China Univ. Geosci.* **1998**, *23*, 438–442.
5. Lu, S.N.; Chen, Z.H.; Li, H.K.; Hao, G.J.; Zhou, H.Y.; Xiang, Z.Q. Mesoproterozoic (early) geological evolution of Qinling orogenic belt. *Geol. Bull. China* **2004**, *23*, 107–112.
6. Lu, S.N.; Yu, H.F.; Li, H.K.; Chen, Z.H.; Wang, H.C.; Xiang, Z.Q. Overview of Paleozoic suture zone and tectonic zoning of the Central Orogenic Belt. *Geol. Bull. China* **2006**, *25*, 1368–1380.
7. Fu, C.L.; Yan, Z.; Wang, Z.Q.; Solomon, B.; Jonathan, A.; Niu, M.L.; Gao, B.; Guo, X.Q.; Li, X.C.; Li, Y.S.; et al. Lajishankou Ophiolite Complex: Implications for Paleozoic Multiple Accretionary and Collisional Events in the South Qilian Belt. *Tectonics* **2018**, *37*, 1321–1346. [CrossRef]
8. Fu, C.L.; Yan, Z.; Buchman, S.; Aitchison, J.; Niu, M.L. The origin and emplacement of the Lajishankou ophiolite complex in the South Qilian belt: Evidences from geological mapping. *Acta Geol. Sin. Engl. Ed.* **2018**, *92*, 9. [CrossRef]
9. Fu, C.L.; Yan, Z.; Aitchison, J.C.; Xiao, W.J.; Buckman, S.; Wang, B.Z.; Zhai, Q.G. Relicts of a Cambrian oceanic arc in the Lajishan suture, NE Tibetan Plateau: Evidence for early-stage subduction within the Proto-Tethyan Ocean. *Palaeogeogr. Palaeoclimatol. Palaeoecol.* **2022**, *585*, 110713. [CrossRef]
10. Fu, C.L.; Yan, Z.; Guo, X.Q.; Niu, M.L.; Cao, B.; Wu, Q.; Li, X.C.; Wang, Z.Q. Assembly and dispersal history of continental blocks within the Altun-Qilian-North Qaidam mountain belt, NW China. *Int. Geol. Rev.* **2019**, *61*, 424–447. [CrossRef]
11. Xu, Z.Q.; Yang, J.S.; Li, H.B.; Yao, J.X. Early Paleozoic terrane framework and formation of high pressure/ultra-high pressure metamorphic belt in central orogenic belt. *Acta Geol. Sin.* **2006**, *80*, 1793–1806.
12. Xu, Z.Q.; Yang, J.S.; Li, H.Q.; Wang, R.R.; Cai, Z.H. Indochinese collisional orogenic system and its orogenic mechanism in Mainland China. *Acta Petrol. Sin.* **2012**, *28*, 1697–1709.
13. Xu, Z.Q.; Yang, J.S.; Li, W.C.; Li, H.H.; Cai, Z.H.; Yan, Z.; Ma, C.Q. Paleo-tethys system and accretive orogeny in the Tibetan Plateau. *Acta Petrol. Sin.* **2013**, *29*, 1847–1860.
14. Pan, G.T.; Wang, L.Q.; Li, R.S.; Yuan, S.H.; Ji, W.H.; Yin, F.G.; Zhang, W.P.; Wang, B.D. Tectonic evolution of the Qinghai-Tibet Plateau. *J. Asian Earth Sci.* **2012**, *53*, 3–14. [CrossRef]
15. Xu, Z.Q.; Yang, J.S.; Wu, C.L.; Li, H.B.; Zhang, J.X.; Qi, X.X.; Song, S.G.; Qiu, H.J. Timing and mechanism of formation and exhumation of the Northern Qaidam ultrahigh pressure metamorphic belt. *J. Asian Earth Sci.* **2006**, *28*, 160–173.
16. Wu, C.L.; Persing, H.; Meibom, A.; Yang, J.S.; Xu, Z.Q.; Wooden, J.L.; Ireland, T.; Li, H.B.; Shi, R.D.; Meng, F.C.; et al. Granitic magmatism in the Paleozoic ultra-high pressure belt in the northern margin of Qaidam Basin. *Acta Geol. Sin.* **2004**, *78*, 658–674.
17. Wu, C.L.; Gao, Y.H.; Wu, S.P.; Chen, Q.L.; Wooden, J.L.; Mazadab, F.K.; Mattinson, C. SHRIMP dating of Paleozoic granites in Daqaidan area, northern margin of Qaidam Basin. *Acta Petrol. Sin.* **2007**, *23*, 1861–1875.
18. Wu, C.L.; Wooden, J.L.; Robinson, P.T.; Gao, Y.H.; Wu, S.P.; Chen, Q.L.; Mazdab, F.K.; Mattinson, C. Geochemistry and zircon SHRIMP U-Pb dating of granitoids from the west segment in the North Qaidam. *Sci. China Ser. D Earth Sci.* **2009**, *52*, 1771–1790. [CrossRef]
19. Wu, C.L.; Gao, Y.H.; Li, Z.L.; Lei, M.; Qin, H.P.; Li, M.Z.; Liu, C.H.; Frost, R.B.; Robinson, P.T.; Wooden, H.L. Zircon SHRIMP U-Pb dating of granites from Dulan and the chronological framework of the North Qaidam UHP belt, NW China. *Sci. China Ser. D Earth Sci.* **2014**, *57*, 2945–2965. [CrossRef]
20. Yang, J.S.; Xu, Z.Q.; Song, S.G.; Zhang, J.X.; Wu, C.L.; Shi, R.D.; Li, H.B.; Brunel, M.; Tapponnier, P. Subduction of continental crust in the early palaeozoic North Qaidam ultrahigh-pressure metamorphic belt, NW China: Evidence from the discovery of coesite in the belt. *Acta Geol. Sin. Engl. Ed.* **2002**, *76*, 63–68.
21. Yang, J.S.; Xu, Z.Q.; Zhang, J.X.; Song, S.G.; Wu, C.L.; Shi, R.D.; Li, H.B.; Brunel, M. Early Palaeozoic North Qaidam UHP metamorphic belt on the north-eastern Tibetan plateau and a paired subduction model. *Terra Nova.* **2002**, *14*, 397–404.
22. Song, S.G.; Niu, Y.L.; Su, L.; Zhang, C.; Zhang, L.F. Continental orogenesis from ocean subduction, continental collision/subduction, to orogen collapse, and recycling: The example of the North Qaidam UHPM belt, NW China. *Earth Sci. Rev.* **2014**, *129*, 59–84. [CrossRef]
23. Yang, J.J.; Zhu, H.; Deng, J.F.; Zhou, T.Z.; Lai, S.C. Discovery of garnet peridotite in the northern margin of Qaidam and its significance. *Acta Petrol. Mineral.* **1994**, *13*, 97–105.
24. Yang, J.S.; Xu, Z.Q.; Song, S.G.; Zhang, J.X.; Wu, C.L.; Shi, R.D.; Li, H.B.; Brunel, M. Discovery of coesite in the North Qaidam Early Palaeozoic ultrahigh pressure (UHP) metamorphic belt, NW China. *Comptes Rendus Acad. Sci. Ser. IIA Earth Planet. Sci.* **2001**, *333*, 719–724. [CrossRef]
25. Zhang, J.X.; Yang, J.S.; Mattinson, C.G.; Xu, Z.Q.; Meng, F.C.; Shi, R.D. Two constrasting eclogite cooling histories, North Qaidam HP/UHP terrane, western China: Petrological and isotopic constraints. *Lithos* **2005**, *84*, 51–76. [CrossRef]

26. Zhang, J.X.; Yang, J.S.; Meng, F.C.; Wan, Y.S.; Li, H.M.; Wu, C.L. U-Pb isotopic studies of eclogites and their host gneisses in the Xitieshan area of the North Qaidam Mountains, western China: New evidence for an early Paleozoic HP-UHP metamorphic belt. *Asian Earth Sci.* **2006**, *28*, 143–150.
27. Song, S.G.; Zhang, C.; Li, X.H.; Zhang, L.F. Metamorphic age of middle tinite eclogite in the ultra-high pressure belt in the northern margin of Qaidam. *Acta Petrol. Sin.* **2011**, *27*, 1191–1197.
28. Xia, L.Q.; Li, X.M.; Yu, J.Y.; Wang, G.Q. Volcanism and tectonic evolution in Mid-Late Neoproterozoic to Early Paleozoic in Qilian Mountains. *Geol. China* **2016**, *43*, 1087–1138.
29. Shi, R.D.; Yang, J.S.; Wu, C.L.; Iizuka, T.; Hirata, T. Island arc volcanic rocks in the ultra-high pressure metamorphic belt in the northern margin of Qaidam. *Acta Geol. Sin.* **2004**, *78*, 52–64.
30. Zhang, Z.W.; Li, W.Y.; Gao, Y.B.; Zhang, J.W.; Guo, Z.P.; Li, K. Zircon U-Pb age of ID-TIMS from Yulonggou Pluton in South Qilian and its geological significance. *Geol. Bull. China* **2012**, *31*, 455–462.
31. Zhang, Z.W.; Li, W.Y.; Gao, Y.B.; Zhang, J.W.; Guo, Z.P.; Li, K.; Wang, Y.L.; Qian, B. Discussion on the formation age and mechanism of Yakqu Nickel-copper basic-complex in South Qilian. *Acta Geosci. Sin.* **2012**, *33*, 92–935.
32. Zhang, Z.W.; Li, W.Y.; Wang, Y.L.; Gao, Y.B. Genesis of basic-ultrabasic pluton in Xiashitang Cu-Ni deposit, Hualong area, South Qilian: Zircon chronology, geochemistry and Sr-Nd isotope constraints. *Acta Petrol. Sin.* **2015**, *31*, 2539–2548.
33. Zhang, Z.W. Geological and Geochemical Characteristics of Mafic-Ultramafic Intrusive Rocks and Cu-Ni Mineralization in Hualong Area, South Qilian. Ph.D. Thesis, Chang'an University, Xi'an, China, 2015; pp. 1–178.
34. Yong, Y.; Xiao, W.J.; Yuan, C.; Yan, Z.; Li, J.L. Geochronology and geochemistry of Paleozoic granites in the eastern part of Middle Qilian and their tectonic implications. *Acta Petrol. Sin.* **2008**, *24*, 855–866.
35. Yang, H.; Zhang, H.F.; Luo, B.J.; Gao, Z.; Guo, L.; Xu, W.C. Generation of peraluminous granitic magma in a post-collisional setting: A case study from the eastern Qilian orogen, NE Tibetan Plateau. *Gondwana Res.* **2016**, *36*, 28–45. [CrossRef]
36. Guo, Z.P.; Li, W.Y.; Zhang, Z.W.; Gao, Y.B.; Zhang, J.E.; Li, K.; Kong, H.L.; Qian, B. Petrogenesis of Lumanshan granite in South Qilian area; Geochemistry, zircon U-Pb chronology and Hf isotope constraints. *Geol. China* **2015**, *42*, 864–880.
37. Yan, Z.; Wang, Z.Q.; Li, J.L.; Xu, Z.Q.; Deng, J.F. Tectonic properties and accretive orogeny of the West Qinling Wedge. *Acta Petrol. Sin.* **2012**, *6*, 1808–1828.
38. Yan, Z.; Aitchison, J.; Fu, C.L.; Guo, X.Q.; Niu, M.L.; Xia, W.J.; Li, J.L. Hualong Complex, South Qilian terrane: U-Pb and Lu-Hf constraints on Neoproterozoic micro-continental fragments accreted to the northern Proto-Ththyan margin. *Precambrian Res.* **2015**, *266*, 65–85. [CrossRef]
39. Wan, Y.S.; Yang, J.S.; Xu, Z.Q.; Wu, C.L. Geochemical characteristics of the Maxianshan compiex and Xinglongshan Group in the eastern segment of the Qilian orogenic belt. *J. Geol. Soc. China* **2000**, *43*, 52–68.
40. Xu, Z.Q.; Yang, J.S.; Wu, C.L.; Li, H.B.; Zhang, J.X.; Qi, X.X.; Song, S.G.; Wan, Y.S.; Chen, W.; Qiu, H.J. Time limit and mechanism of formation and reentry of ultra-high pressure metamorphic belt in the northern margin of Qaidam. *Acta Geol. Sin.* **2003**, *77*, 163–176.
41. Li, W.Y. Metallogenesis and Prospecting of Sulfide Metal Deposit in Qilian Mountain Magmatism. Ph.D. Thesis, Northwestern University, Xi'an, China, 2004; pp. 1–188.
42. Gao, Y.B.; Li, W.Y.; Xie, X.; Zhang, Z.W.; Guo, Z.P.; Zhang, J.W.; Li, K. Geology, geochemistry and genesis of Lashuixia Cu-Ni deposit in Hualong area, Qinghai Province. *Geol. Bull. China* **2012**, *31*, 763–772.
43. Xu, W.C.; Zhang, H.F.; Liu, X.M. Zircon U-Pb dating limits the formation age and tectonic significance of high-grade metamorphic rock series in the Qilian Mountains. *Chin. Sci. Bull.* **2007**, *52*, 1174–1180.
44. He, S.P.; Li, R.S.; Wang, C.; Yu, P.S.; Zhang, H.F.; Gu, P.Y.; Shi, C. Further definition of the formation age of Hualong Group in the eastern section of South Qilian. *Acta Petrol. Mineral.* **2011**, *30*, 34–44.
45. Yu, J.Y.; Li, X.M.; Ma, Z.P.; Tang, Z.; Wang, G.Q.; Sun, J.M.; Wu, P. LA-ICP-MS Zircon U-Pb age of Hualong Group in South Qilian and its geological significance. *Northwest. Geol.* **2012**, *45*, 79–85.
46. Fu, C.L.; Yan, Z.; Guo, X.Q.; Niu, M.L.; Xia, W.J.; Wang, Z.Q.; Li, J.L. Geochemical characteristics and SHRIMP zircon U-Pb ages of diabase from ophiolite melanges in the Laji Mountain Pass. *Acta Petrol. Sin.* **2014**, *6*, 1695–1706.
47. Yang, J.H.; Du, Y.S.; Cawood, P.A.; Xu, Y.J. From Subduction to Collision in the Northern Tibetan Plateau: Evidence from the Early Silurian Clastic Rocks, Northwestern China. *J. Geol.* **2012**, *120*, 50–68. [CrossRef]
48. Ma, H.S.; Mao, J.H.; Zhou, Z.H. The Geology of Qilian Mountain. In *Geological Atlas of China*; Ma, L.F., Ed.; Geological Publishing House: Beijing, China, 2002; pp. 89–91.
49. Yuan, H.L.; Gao, S.; Liu, X.M. Accurate U-Pb age and trace element determinations of zircon by laser ablation inductively coupled plasma mass spectrometry. *Geostand. Geoanal. Res.* **2004**, *28*, 353–370. [CrossRef]
50. Andersen, T. Correction of common Pb in U-Pb analyses that do not report ^{204}Pb. *Chem. Geol.* **2002**, *192*, 59–79. [CrossRef]
51. Ludwig, K. *Isoplot/Ex 2. 49: A Geochronological Toolkit for Microsoft Excel*; Special Publication, No. 1a; Berkeley Geochronology Center: Berkeley, CA, USA, 2001.
52. Corfu, F.; Hanchar, J.M.; Hoskin, P.W.O.; Kinny, P. Atlas of zircon textures. *Rev. Mineral. Geochem.* **2003**, *53*, 469–500. [CrossRef]
53. Zhang, Y.M.; Pei, X.Z.; Li, Z.C.; Li, R.B.; Liu, C.J.; Pei, L.; Chen, Y.X.; Chen, G.C.; Wang, M.; Ling, G.C. LA-ICP-MS Zircon U-Pb Dating and Geochemistry of the Dangjiasi Granitic Complex in the Qinghai Nanshan Tectonic Zone, and Its Geological Implication. *Acta Geol. Sin.* **2017**, *91*, 19.

54. Zhang, X.Y.; Li, W.F.; Liu, J.D.; Ouyang, G.W.; Wang, C.T. Identification and geological significance of Early Ordovician Adakite in Xiamen, eastern section of Lajishan Hybrid Belt. *Northwest. Geol.* **2020**, *53*, 18.
55. Frost, B.R.; Arculus, R.J.; Barnes, C.G.; Collins, W.J.; Ellis, D.J.; Frost, C.D. A geochemical classification of granitic rocks. *Petrology* **2001**, *42*, 2033–2048. [CrossRef]
56. Rickwood, P.C. Boundary lines within petrologic diagrams which use oxides of major and minor elements. *Lithos* **1989**, *22*, 247–263. [CrossRef]
57. Halyard, M.; Nielsen, R.L.; Beard, J.S.; Douce, A.P.; Blencoe, J. Experimental determination of the partitioning behavior of rare earth and high field strength elements between pargasitic amphibole and natural silicate melts. *Geochim. Cosmochim. Acta* **2000**, *64*, 1103–1120. [CrossRef]
58. Defant, M.J.; Drummond, M.S. Derivart ion of some modern arc magmas by melting of young subduction lithosphere. *Nature* **1990**, *347*, 662–665. [CrossRef]
59. Kay, R.W.; Kay, S.M. Delamination and delamination magmatism. *Tectonophysics* **1993**, *219*, 177–189. [CrossRef]
60. Stern, C.R.; Kilian, R. Role of the subducted slab, mantle wedge and continental crust in the generation of adakites from the Austral Volcanic Zone. *Contrib. Mineral. Petrol.* **1996**, *123*, 263–281. [CrossRef]
61. Drummond, M.S.; Defant, M.J.; Kepezhinskas, P.K. The petrogenesis of slab derived trondhjemite-tonalite- dacite/adakite magmas. *Trans. R Soc. Edinburg Earth Sci.* **1996**, *87*, 205–216.
62. Sajona, F.G.; Maury, R.C.; Pubellier, M.; Leterrier, J.; Bellon, H.; Cotton, J. Magmatic source enrichment by slab-derived melts in a young post-collision setting, central Min-danao. *Lithos* **2000**, *54*, 173–206. [CrossRef]
63. Defant, M.J.; Drummond, M.S.; Mount, S.T. Potential example of the partial melting of the subducted lithosphere in a volcanic arc. *Geology* **1993**, *21*, 547–550. [CrossRef]
64. Martin, H.; Smithies, R.H.; Rapp, R.; Moyen, J.F.; Champion, D. An overview of adakite, tonalite-trondhjemite-granodio-rite (TTG), and sanukitoid: Relationships and some implications for crustal evolution. *Lithos* **2005**, *79*, 1–24. [CrossRef]
65. Maniar, P.D.; Piccoli, P.M. Tectonic discrimination of granitoids. *Geol. Soc. Am. Bull.* **1989**, *101*, 635–643. [CrossRef]
66. Zhang, L.Y.; Li, S.C.; Zhao, Q.Y. A review of research on adakites. *Int. Geol. Rev.* **2019**. [CrossRef]
67. Castillo, P.R.; Janney, P.E.; Solidum, R.U. Petrology and geochemistry of Camiguin island, southern Philippines: Insights to the source of adakites and other lavas in a complex arc set-ting. *Contrib. Miner. Petrol.* **1999**, *134*, 33–51. [CrossRef]
68. Chappell, B.W.; White, A.J.R. I- and S-type granites in the Lachlan Fold Belt. Transactions of the Royal Society of Edinburgh. *Earth Sci.* **1992**, *83*, 1–26.
69. Rollison, H.R. *Using Geochemical Data: Evaluation, Presentation, Interpretation*; Routledge: Oxfordshire, UK, 2014.
70. Boynton, W.V. Geochemistry of the rare earth elements; Meteorite studies. In *Rare Earth Element Geochemistry*; Henderson, P., Ed.; Elsevier: Amsterdam, The Netherlands, 1984; pp. 63–114.
71. Sun, S.S.; McDonough, W.F. Chemical and isotopic systematics of oceanic basalts; Implications for mantle composition and processes. In *Magmatism in the Ocean Basins*; Sunders, A.D., Norry, M.J., Eds.; The Geological Society of London: London, UK, 1989; Volume 42, pp. 313–345.
72. Atherton, M.P.; Petford, N. Generation of sodium-rich magmas from newly underplated basaltic crust. *Nature* **1993**, *362*, 144–146. [CrossRef]
73. Condie, K.C. TTGs and adakites: Are they both slab melts? *Lithos* **2005**, *80*, 33–44. [CrossRef]
74. Xu, J.F.; Shinjio, R.; Defant, M.J.; Qiang, W.; Rapp, R.P. Origin of Mesozoic adakitic intrusive rocks in the Ningzhen area of east China: Partial melting of delaminated lower continental crust? *Geology* **2002**, *30*, 1111–1114. [CrossRef]
75. Gao, S.; Rudnick, R.L.; Yuan, H.L.; Wang, Q.H. Recycling lower continental crust in the North China craton. *Nature* **2004**, *432*, 892–897. [CrossRef] [PubMed]
76. Wang, Q.; Xu, J.F.; Jian, P.; Bao, Z.W.; Zhao, Z.H.; Li, C.F.; Xiong, X.L.; Ma, J.L. Petrogenesis of adakitic porphyries in an extensional tectonic setting, Dexing, South China: Implications for the genesis of porphyry copper mineralization. *J. Petrol.* **2006**, *47*, 119–144. [CrossRef]
77. Qian, Q. Geochemical characteristics and genesis of adakite. *Acta Petrol. Mineral.* **2001**, *20*, 297–306.
78. Defant, M.J.; Kepezhinskas, P. Evidence suggests slab melting in arc magmas. *EOS Trans. Am. Geophys. Union* **2001**, *82*, 62–70. [CrossRef]
79. Taylor, S.R.; McLennan, S. The geochemical composition of the continental crust. *Rev. Geophys.* **1995**, *33*, 241–265. [CrossRef]
80. Kaygusuz, A.; Siebel, W.; Sen, C.; Satir, M. Petrochemistry and petrology of I-type granitoids in an arc setting; the composite Torul pluton, Eastern Pontides, NE Turkey. *Int. J. Earth Sci.* **2008**, *97*, 739–764. [CrossRef]
81. Hofmann, A.W. Chemical differentiation of the Earth; the relationship between mantle, continental crust, and oceanic crust. *Earth Planet. Sci. Lett.* **1988**, *90*, 297–314. [CrossRef]
82. Patiño Douce, A.E. *What Do Experiments Tell Us about the Relative Contributions of Crust and Mantle to the Origin of Granitic Magmas*; Geological Society Special Publications: London, UK, 1999; Volume 168, pp. 55–75.
83. Wang, H.C.; Lu, S.N.; Yuan, G.B.; Xin, H.Y.; Zhang, B.H.; Wang, Q.H.; Tian, Q. Tectonic properties and formation age of Tanjianshan Group in the northern margin of Qaidam Basin. *Geol. Bull. China* **2003**, *22*, 487–493.
84. Huang, Z.B.; Zhen, J.P.; Li, B.H.; Qi, W.; Wei, Z.J.; Chen, X. Geochronology and Geochemistry of Early Paleozoic backarc basin ophiolite in Erji, South Qilian Avenue and its significance. *Geotecton. Metallog.* **2016**, *40*, 826–838.

85. Whalen, J.B.; Hildebrand, R.S. Trace element discrimination of arc, slab failure, and a-type granitic rocks. *Lithos* **2019**, *348–349*, 105179. [CrossRef]
86. Christiansen, E.H.; Keith, J.D. Trace element systematics in silicic magmas: A metallogenic perspective. In *Geological Association of Canada Short Course Notes Volume 12, Trace Element Geochemistry of Volcanic Rocks*; Geological Association of Canada: Winnipeg, MB, Canada, 1996; pp. 115–151.
87. Peacock, S.M.; Rushmer, T.; Thompson, A.B. Partial melting of subducting oceanic crust. *Earth Planet. Sci. Lett.* **1994**, *121*, 227–244. [CrossRef]
88. Brenan, J.M.; Shaw, H.F.; Ryerson, F.J. Experimental determination fo trace-element partitioning between pargasite and a synthetic hydrous andesitic melt. *Earth Planet. Sci. Lett.* **1995**, *135*, 1–11. [CrossRef]
89. Drummond, M.S.; Defant, M.J. A model for trondhjemite-tonalite-dacite genesis and crustal growth via slab melting: Archean to modern comparisons. *J. Geophys. Res.* **1990**, *95*, 21503–21521. [CrossRef]
90. Saunders, A.D. The rare earth element characteristics of igneous rocks from the ocean basins. In *Developments in Geochemistry*; Elsevier: Amsterdam, The Netherlands, 1984; Volume 2, pp. 205–236.
91. Pearce, J.A. Sources and settings granitic rocks. *Episoders* **1996**, *19*, 120–125. [CrossRef]
92. Pearce, J.A.; Harris NB, W.; Tindle, A.G. Trace element discrimination diagrams for the tectonic inter pretation of granitic rocks. *J. Petrol.* **1984**, *25*, 956–983. [CrossRef]
93. Li, S.Z.; Zhao, S.J.; Yu, S.; Cao, H.H.; Li, X.Y.; Liu, X.; Guo, X.Y.; Xiao, W.J.; Lai, S.C. Proto-tethyan Ocean of East Asia (II); Affinity and aggregation of early Paleozoic microlandmasses. *Acta Petrol. Sin.* **2016**, *32*, 2628–2644.
94. Xia, X.H.; Song, S.G.; Niu, Y.L. Tholeiite-Boninite terrane in the North Qilian suture zone; Implicationgs for subductiong initiation and back-arc basin development. *Chem. Geol.* **2012**, *328*, 259–277. [CrossRef]
95. Wu, C.L.; Yao, S.Z.; Yang, J.S.; Zeng, L.S.; Chen, Y.S.; Li, H.B.; Qi, X.X.; Wooden, J.L.; Mazdab, F.K. Granite evidence for Early Paleozoic bidirectional subduction in the Northern Qilian Ocean. *Geol. China* **2006**, *33*, 1197–1208.
96. Zhao, Z.X.; Wei, J.H.; Fu, L.B.; Liang, S.N.; Zhao, S.Q. The Early Paleozoic Xitieshan syn-collisional granite in the North Qaidam ultrahigh-pressure metamorphic belt, NW China: Petrogenesis and implications for continental crust growth. *Lithos* **2017**, *278*, 140–152. [CrossRef]